

Study of one-step and two-step neutron transfer in the reaction ${}^6\text{Li} + {}^9\text{Be}^*$

A.K. Azhibekov^{1,2} S.M. Lukyanov¹ Yu.E. Penionzhkevich^{1,3} B.A. Urazbekov⁴ M.A. Naumenko¹
 V.V. Samarin^{1,5} T. Issatayev^{1,4,6} V.A. Maslov¹ K. Mendibayev^{1,6} D. Aznabayev¹
 T.K. Zholdybayev⁶ A. Temirzhanov^{6,7}

¹Joint Institute for Nuclear Research, Dubna, Russia

²Korkyt Ata Kyzylorda University, Kyzylorda, Kazakhstan

³National Research Nuclear University MEPhI, Moscow, Russia

⁴L.N. Gumilyov Eurasian National University, Astana, Kazakhstan

⁵Dubna State University, Dubna, Russia

⁶Institute of Nuclear Physics, Almaty, Kazakhstan

⁷Satbayev University, Almaty, Kazakhstan

Abstract: This paper presents the results of experiments conducted to measure the cross-sections for elastic scattering and nucleon transfer channels in the ${}^6\text{Li}+{}^9\text{Be}$ reaction at an incident energy of 68 MeV: ${}^9\text{Be}({}^6\text{Li}, {}^6\text{Li}){}^9\text{Be}$, ${}^9\text{Be}({}^6\text{Li}, {}^7\text{Li}){}^8\text{Be}$, ${}^9\text{Be}({}^6\text{Li}, {}^7\text{Li}){}^8\text{Be}_{2+}$, ${}^9\text{Be}({}^6\text{Li}, {}^8\text{Li}){}^7\text{Be}$, and ${}^9\text{Be}({}^6\text{Li}, {}^7\text{Be}){}^8\text{Li}$. The objective of the study is to elucidate the manifestation of the cluster structure of ${}^9\text{Be}$. Theoretical analysis of the contributions of the one-step and two-step neutron transfer mechanisms is performed using the distorted wave Born approximation method with the Fresco code. Good agreement between the calculations and the experimental data is obtained for the channels of elastic scattering ${}^9\text{Be}({}^6\text{Li}, {}^6\text{Li}){}^9\text{Be}$, neutron ${}^9\text{Be}({}^6\text{Li}, {}^7\text{Li}){}^8\text{Be}$, and proton transfer ${}^9\text{Be}({}^6\text{Li}, {}^7\text{Be}){}^8\text{Li}$, as well as for the transfer of two neutrons ${}^9\text{Be}({}^6\text{Li}, {}^8\text{Li}){}^7\text{Be}$. The dineutron cluster transfer mechanism makes a dominant contribution to the ${}^9\text{Be}({}^6\text{Li}, {}^8\text{Li}){}^7\text{Be}$ reaction channel at forward angles.

Keywords: elastic scattering, neutron and proton transfer, reaction mechanisms, DWBA, Fresco code

DOI: 10.1088/1674-1137/ad6d40

I. INTRODUCTION

The study of one-step and two-step transfer of nucleons and clusters in nuclear reactions may answer the question of the existence of multi-neutron systems, which is an important problem in nuclear physics. The problem of the existence of light neutron clusters (dineutron, tetraneutron, *etc.*) is over 60 years old, but it is still of interest for both theoretical and experimental studies [1–5]. A recent paper [6] reported that the observation of a resonance structure near the threshold for the formation of a four-neutron system corresponds to a quasi-bound tetraneutron cluster that manifests itself in the ${}^8\text{He}+p\rightarrow{}^4\text{He}+p+{}^4n$ reaction and lives for a very short time.

Concerning the problem of studying light neutron clusters, a dineutron is of great interest. The dineutron can be formed near the surface of neutron-rich nuclei [7]. The first attempt to observe an unstable dineutron, *i.e.*, a system of two neutrons in the singlet state, was made by V. K. Voitovetskii *et al.* in reaction ${}^2\text{H}(n,p){}^2n$ at $E_n = 14$ MeV from the spectrum of the protons [8]. In Ref. [9],

the authors studied the decay of the ${}^{16}\text{Be}$ nucleus and obtained results that show the dineutron nature of the decay with a small angle of emission between two neutrons. The measured two-neutron separation energy for ${}^{16}\text{Be}$ was 1.35 MeV, which is consistent with calculations in the shell model. However, in these calculations, the authors did not take into account the interaction between the emitted neutrons, which can also explain the observed correlations of the emission angles of the two neutrons [10].

Two-neutron transfer reactions are a unique tool for studying the interaction between neutrons and confirming the existence of the dineutron clusters that manifest themselves during the interaction of two nuclei [11–15]. The difficulty in interpreting experimental data is that such reactions can proceed as both one-step and two-step neutron transfer processes, which cannot be separated experimentally [16]. In Ref. [17], the authors showed that the product nuclei are formed as a result of one-step transfer of two neutrons and that the contribution of this

Received 7 May 2024; Accepted 8 August 2024; Published online 9 August 2024

* Supported by the Science Committee of the Ministry of Science and Higher Education of the Republic of Kazakhstan (AP19677087) and by the Russian Science Foundation (24-22-00117)

† E-mail: kayrat1988@bk.ru

©2024 Chinese Physical Society and the Institute of High Energy Physics of the Chinese Academy of Sciences and the Institute of Modern Physics of the Chinese Academy of Sciences and IOP Publishing Ltd. All rights, including for text and data mining, AI training, and similar technologies, are reserved.

process is especially significant when low-lying excited states are populated in the formed nuclei. Thus, to describe experimental data, it is extremely important to take into account the probabilities of both one-step and two-step neutron transfer [18].

In the elastic scattering of ${}^6\text{He}$ nuclei on ${}^4\text{He}$ [19–22] and ${}^4\text{He}$ on ${}^6\text{Li}$ [23], an increase in the cross-section at backward angles was observed. The authors interpreted this increase as the existence of the dineutron cluster in the ${}^6\text{He}$ nucleus and the deuteron cluster in the ${}^6\text{Li}$ nucleus. However, the optical model of elastic scattering could not describe this effect, while the calculation of the corresponding transfer cross-sections for dineutron and deuteron clusters within the framework of the distorted wave Born approximation (DWBA) method fully explained this behavior as the contribution of the channel of the transfer of a two-nucleon cluster.

Another interesting experimental result was obtained in Ref. [24] for the ${}^6\text{He}+{}^{65}\text{Cu}$ reaction at a beam energy of 22.6 MeV: the cross-section for the two-neutron transfer was found to be larger than that for one-neutron transfer. Thus, the authors concluded that “the dineutron configuration of ${}^6\text{He}$ plays a dominant role in the reaction mechanism.”

Concerning the ${}^9\text{Be}$ nucleus, it was revealed that the dineutron cluster manifests itself in the reaction channel ${}^9\text{Be}({}^3\text{He}, {}^7\text{Be}){}^5\text{He}$ [25, 26]. The ${}^9\text{Be}({}^3\text{He}, {}^6\text{He}){}^6\text{Be}$ reaction channel observed at forward angles corresponds to the transfer of three neutrons. The calculations reported in [25] within the framework of the coupled reaction channels (CRC) method showed that the two-step transfer mechanisms (n - $2n$ and $2n$ - n) make a significant contribution to the cross-section, which is also an indirect evidence of the transfer of the dineutron cluster.

The present study is a part of our systematic studies of nucleon and cluster transfer in reactions with various projectiles on ${}^9\text{Be}$: $d+{}^9\text{Be}$ [27] and ${}^3\text{He}+{}^9\text{Be}$ [25, 26]. Here, we studied reaction channels with the weakly bound projectile nucleus ${}^6\text{Li}$. The aim was to elucidate the manifestation of the cluster structure of ${}^9\text{Be}$ in the studied reaction channels. In particular, we focused on the reaction channel ${}^9\text{Be}({}^6\text{Li}, {}^8\text{Li}){}^7\text{Be}$ to estimate whether a one-step or two-step transfer is the most probable mechanism of the transfer of two neutrons.

Section II provides a detailed description of the conducted experiment. Section III presents experimental cross-sections and their comparative analysis. Sections IV and V are devoted to the theoretical method employed to analyze the experimental data. Sections VI and VII present the results of the theoretical analysis of the experimental data.

II. EXPERIMENT

The experiment was performed at the Flerov Laborat-

ory of Nuclear Reactions, Joint Institute for Nuclear Research, Dubna. An intense ${}^6\text{Li}$ beam with an energy of 68 MeV was accelerated by the U-400 cyclotron and transported to the reaction chamber (Fig. 1) of the high-resolution magnetic analyzer MAVR [28].

The beam profile was formed by the magnetic optics of the U-400 cyclotron supplemented by a system of diaphragms. The beam size was controlled by the profilometer installed in front of the reaction chamber; on a target, it was $5\text{ mm} \times 5\text{ mm}$ at an intensity of 30 nA. The total number of particles passing through the target was determined by a Faraday cup and also monitored by elastic scattering.

The beam was focused onto the self-supporting $5\text{-}\mu\text{m}$ thick ${}^9\text{Be}$ foil. The target purity was higher than 99%; a possible admixture of carbon and oxygen isotopes in the target material was not observed in the measured energy spectra.

Particle identification was done by measuring energy losses and residual energy in detectors (ΔE - E method). For this purpose, three three-layer semiconductor telescopes were used, the first two thin detectors of which measured specific energy losses ΔE_1 , ΔE_2 (Fig. 1). Their thickness was 50 and $300\ \mu\text{m}$, respectively. The third detector E_R was 3.2-mm thick and measured the residual energy of the reaction products after they passed through the first two detectors. The configuration of such telescopes made it possible to reliably identify reaction products from helium to boron isotopes in a wide energy range. Examples of identification matrices obtained by one of the telescopes used in the experiments are shown in Fig. 2. It can be seen that the reaction products were unambiguously identified.

To measure the energy spectra and angular distributions of the nuclei emitted in the reaction, we used an inclusive method. The energy resolution of the detecting system was determined by the energy resolution of the ${}^6\text{Li}$ beam and errors in measuring the energy losses of particles in the target material. In the case of registration of particles with $Z = 1$ –3, the energy resolution was ≈ 500

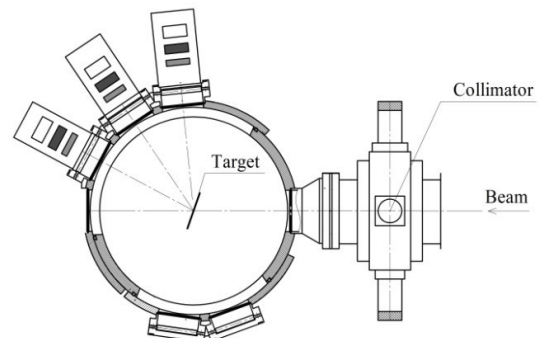


Fig. 1. Reaction chamber with the ${}^9\text{Be}$ foil target and three three-layer semiconductor telescopes (ΔE_1 , ΔE_2 , E_R).

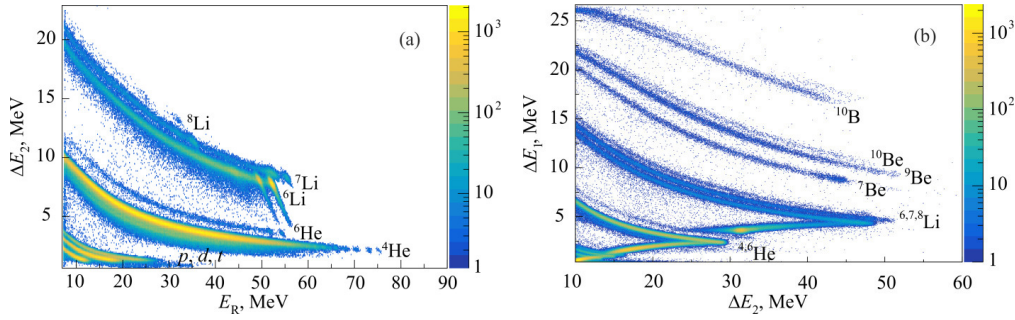


Fig. 2. (color online) Examples of identification matrices obtained by one of the telescopes: (a) $\Delta E_2 - \Delta E_R$ at an angle of $\theta_{\text{lab}} = 16^\circ$ and (b) $\Delta E_1 - \Delta E_2$ at $\theta_{\text{lab}} = 12^\circ$.

keV; for particles with $Z = 4-5$, it was ≈ 1 MeV.

The excitation energy spectra corresponding to the energy of the states of the ${}^9\text{Be}$, ${}^8\text{Be}$, ${}^7\text{Be}$, and ${}^8\text{Li}$ nuclei are shown in Figs. 3 and 4. The populated ground and first excited states are indicated. Note that the width of each peak of a state in the spectra was determined by three factors: natural width, instrument resolution of the spectrometer, and energy spread. Events corresponding to multibody exit channels make insignificant contributions to these peaks. The excited states of the complementary products corresponding to the two-body exit channels can be observed in the resulting energy spectra. The complementary products are as follows:

- ${}^9\text{Be}$ in the reaction channel ${}^9\text{Be}({}^6\text{Li}, {}^6\text{Li}){}^9\text{Be}$ (in the case of detection of ${}^6\text{Li}$ [Fig. 3(a)]);
- ${}^8\text{Be}$ in the reaction channel ${}^9\text{Be}({}^6\text{Li}, {}^7\text{Li}){}^8\text{Be}$ (in the case of detection of ${}^7\text{Li}$ [Fig. 3(b)]);
- ${}^7\text{Be}$ in the reaction channel ${}^9\text{Be}({}^6\text{Li}, {}^8\text{Li}){}^7\text{Be}$ (in the case of detection of ${}^8\text{Li}$) [Fig. 4(a)];
- ${}^8\text{Li}$ in the reaction channel ${}^9\text{Be}({}^6\text{Li}, {}^7\text{Be}){}^8\text{Li}$ (in the case of detection of ${}^7\text{Be}$ [Fig. 4(b)]).

The narrow peak at 2.43 MeV in Fig. 3(a) is the first excited rotational level $5/2^-$ of the ${}^9\text{Be}$ nucleus. The next wide peak corresponds to overlapping of two excited levels ($7/2^-$, 6.38 MeV) and ($9/2^+$, 6.76 MeV) of ${}^9\text{Be}$. The narrow peak at 3.03 MeV in Fig. 3(b) is the first excited rotational level 2^+ of the ${}^8\text{Be}$ nucleus. For the ${}^9\text{Be}$ and ${}^8\text{Be}$ nuclei, the first rotational levels $5/2^-$ and 2^+ are populated with large probabilities. The single-particle excited levels of the ${}^9\text{Be}$ nucleus are not observed because of the small neutron separation threshold (Table 1). For the ${}^7\text{Be}$ nucleus [Fig. 4(a)], the first low-lying single-particle excited level ($1/2^-$, 0.43 MeV) is not separated from the ground state peak, and the second single-particle excited level ($7/2^-$, 4.57 MeV) is observed. Other single-particle excited levels of the ${}^7\text{Be}$ nucleus are not observed because they are above the proton separation threshold (Table 1)

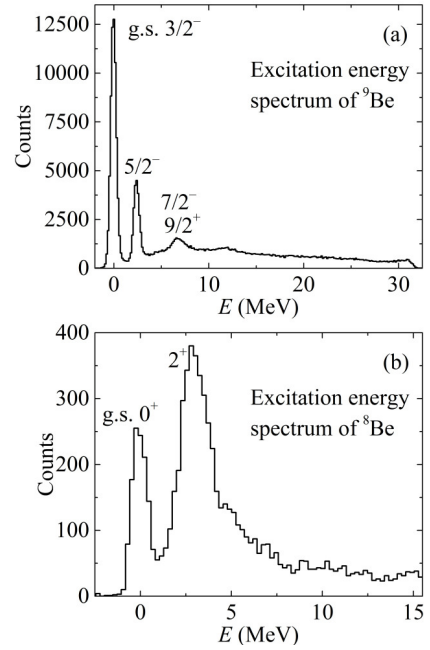


Fig. 3. Excitation energy spectra for (a) ${}^9\text{Be}$ in the case of detection of ${}^6\text{Li}$ at an angle of $\theta_{\text{lab}} = 16^\circ$ and (b) ${}^8\text{Be}$ in the case of detection of ${}^7\text{Li}$ at $\theta_{\text{lab}} = 14^\circ$.

and are populated with low probability. For the ${}^8\text{Li}$ nucleus [Fig. 4(b)], the first low-lying single-particle excited level (1^+ , 0.98 MeV) is situated near the ground state peak. Other single-particle excited levels of the ${}^8\text{Li}$ nucleus are not observed because they are above the neutron separation threshold (Table 1) and are populated with low probability.

III. ANGULAR DISTRIBUTIONS OF REACTION PRODUCTS

Differential cross-sections for each angle were obtained by considering solid angles of the telescopes, the thickness of the target, and the number of particles incident on the target. The experimental setup made it possible to measure the energy spectra of the reaction products in the range of angles 10° – 83° in the laboratory

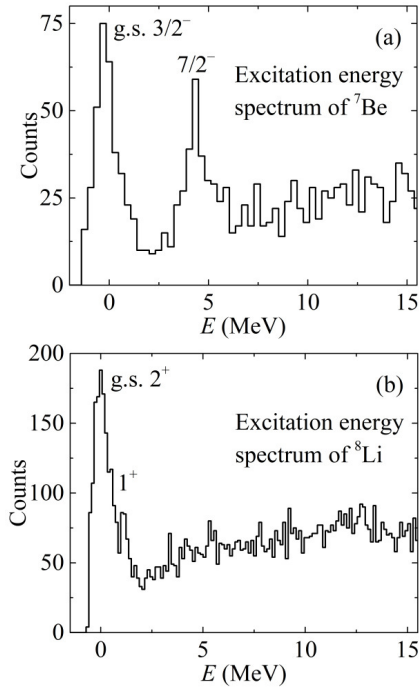


Fig. 4. Excitation energy spectra for (a) ${}^7\text{Be}$ in the case of detection of ${}^8\text{Li}$ at an angle of $\theta_{\text{lab}} = 12^\circ$ and (b) ${}^8\text{Li}$ in the case of detection of ${}^7\text{Be}$ at $\theta_{\text{lab}} = 16^\circ$.

Table 1. Particle separation energies for the ${}^8\text{Li}$ and ${}^{7,8,9}\text{Be}$ nuclei.

Nucleus	Alpha particle α /MeV	Proton p /MeV	Neutron n /MeV
${}^8\text{Li}$	6.1	12.4	2.03
${}^7\text{Be}$	1.59	5.6	10.7
${}^8\text{Be}$	-0.092	17.3	18.9
${}^9\text{Be}$	2.46	16.9	1.66

system; the error in measuring the angle was $\pm 1^\circ$. Angles greater than 83° could not be measured because of the design features of the scattering chamber. The measured angular distributions of the products of the reaction ${}^6\text{Li}+{}^9\text{Be}$ at an energy of 68 MeV are presented in Figs. 5, 6. The relative error in cross-section measurements is not larger than 20%. This error is predominantly due to the following factors: statistical errors in counting events, errors in target thickness determination, inaccuracies in solid angle values, and errors in beam intensity measurements.

The relatively high cross-sections for the transfer of one neutron n from the weakly bound target nucleus ${}^9\text{Be}$ [Fig. 5(a)] can be explained by the manifestation of its cluster structure ($\alpha+n+\alpha$) [27]. The differential cross-sections for the transfer of two neutrons in the reaction channel ${}^9\text{Be}({}^6\text{Li}, {}^8\text{Li}){}^7\text{Be}$ have comparable values with those for the reaction channels of the transfer of one neutron, ${}^9\text{Be}({}^6\text{Li}, {}^7\text{Li}){}^8\text{Be}_{\text{gs}}$ and ${}^9\text{Be}({}^6\text{Li}, {}^7\text{Li}){}^8\text{Be}_{2+}$. As can be seen

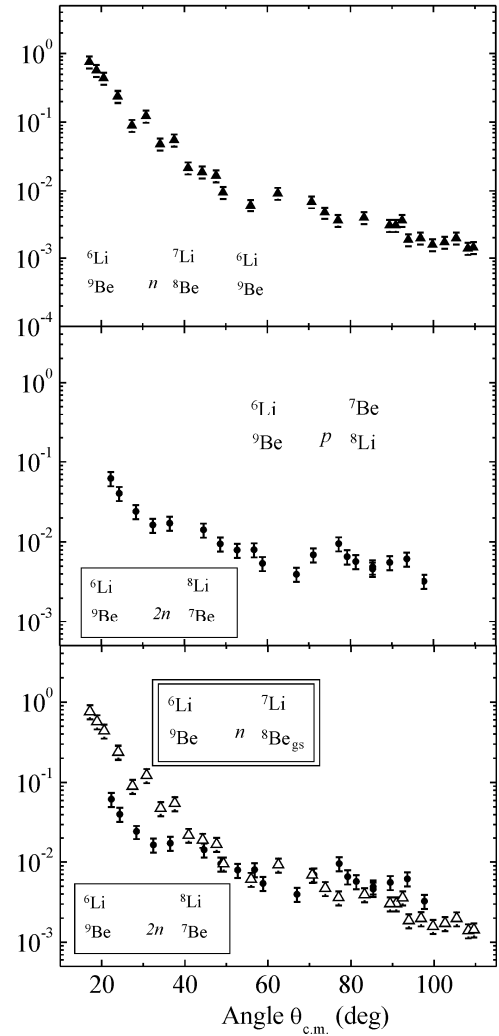


Fig. 5. Experimental angular distributions for the products of the ${}^6\text{Li}+{}^9\text{Be}$ reaction at 68 MeV: (a) ${}^7\text{Li}$ in exit channels ${}^7\text{Li}+{}^8\text{Be}_{\text{gs}}$ (triangles) and ${}^7\text{Li}+{}^8\text{Be}_{2+}$ (circles); (b) ${}^8\text{Li}$ (circles) and ${}^7\text{Be}$ (triangles) in exit channels ${}^8\text{Li}_{\text{gs}}+{}^7\text{Be}_{\text{gs},1/2-}$ and ${}^7\text{Be}_{\text{gs}}+{}^8\text{Li}_{\text{gs},1+}$, respectively; (c) ${}^7\text{Li}$ in exit channel ${}^7\text{Li}+{}^8\text{Be}_{\text{gs}}$ (empty triangles) and ${}^8\text{Li}$ (circles) in exit channel ${}^8\text{Li}_{\text{gs}}+{}^7\text{Be}_{\text{gs},1/2-}$. The transfer mechanisms are shown in insets.

from Fig. 5(c), the ratio σ_{1n}/σ_{2n} for the reaction channels ${}^9\text{Be}({}^6\text{Li}, {}^7\text{Li}){}^8\text{Be}_{\text{gs}}$ and ${}^9\text{Be}({}^6\text{Li}, {}^8\text{Li}){}^7\text{Be}$ at forward angles is approximately equal to 10 and smoothly decreases with increasing angle to ~ 1 .

IV. THEORETICAL ANALYSIS OF ELASTIC SCATTERING

Experimental differential cross-sections for elastic scattering of ${}^6\text{Li}$ on the ${}^9\text{Be}$ nucleus are presented in Fig. 6. The experimental data were analyzed within the optical model using the Fresco code [29, 30]. The optical potential used in the calculations is expressed as

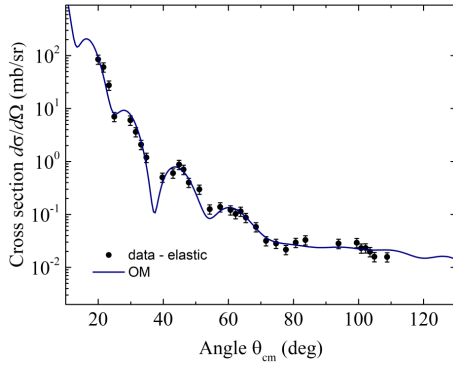


Fig. 6. (color online) Angular distributions for the elastic scattering channel ${}^9\text{Be}({}^6\text{Li}, {}^6\text{Li}){}^9\text{Be}$: experimental data (circles) and results of calculations (curves).

$$U(r) = -V_V f(r; R_V, a_V) - iV_W f(r; R_W, a_W) + V_C(r), \quad (1)$$

with the Woods-Saxon form-factors for both the real and imaginary parts expressed as

$$f(r; R_{V,W}, a_{V,W}) = \{1 + \exp[(r - R_{V,W})/a_{V,W}]\}^{-1}, \quad (2)$$

where

$$R_{V,W} = r_{V,W} (A_p^{1/3} + A_t^{1/3}), \quad (3)$$

V_V and V_W are the depth parameters for the real and imaginary parts of the optical potential, respectively; $r_{V,W}$ and $a_{V,W}$ are geometric parameters; A_p and A_t are the mass numbers of the projectile and target nuclei, respectively; $V_C(r)$ is the Coulomb potential of a uniformly charged sphere with radius

$$R_C = r_C (A_p^{1/3} + A_t^{1/3}). \quad (4)$$

In our calculations, we set $r_C = 0.717$ fm.

The theoretical elastic scattering cross-section was fitted to the measured experimental data within the optical model using the SFresco code [30]. As a starting point for seeking the optical potential in our calculations, we used the parameters for the elastic scattering of ${}^6\text{Li}+{}^9\text{Be}$ at an energy of 50 MeV [31]. All six parameters, namely, depths $V_{V,W}$ and geometric parameters $r_{V,W}$, $a_{V,W}$, were varied. It can be seen that we achieved an excellent fit ($\chi^2/N=1.418$) of the experimental data (Fig. 6). The parameters of the potential expressed by Eq. (1) are listed in

Table 2. Parameters of the optical potential (1) for elastic scattering.

V_V /MeV	r_V /fm	a_V /fm	V_W /MeV	r_W /fm	a_W /fm
152.20	0.698	0.624	12.36	1.388	0.930

Table 2.

V. THEORETICAL ANALYSIS OF TRANSFER CHANNELS

Theoretical analysis of the cross-sections for the transfer channels was performed using the DWBA method [32, 33] and the Fresco code [29, 30]. We calculated the one-step transfer using the prior formalism of the DWBA amplitude. For the two-step transfer of two neutrons, we used the second-order DWBA; a prior-post combination was chosen to avoid non-orthogonality terms [30, 32, 33]. According to the DWBA formalism, the main ingredients required for calculations are the internal wave functions (ϕ_A, ϕ_b) , (ϕ_a, ϕ_B) for the nuclei in the transfer reaction $A+b \rightarrow a+B$ ($A=a+x$, $B=b+x$). The wave function for nucleus B with total spin J and spin projection M can be expressed as [30, 32, 33]

$$\phi_B^{JM}(\xi, r) = \sum_{lj} A_{lsj}^{IJ} [\phi_b^l(\xi) \otimes \varphi_{lsj}(r)]_{JM}, \quad (5)$$

where coefficients A_{lsj}^{IJ} are the so-called coefficients of fractional parentage (CFP) or spectroscopic amplitudes, and their square moduli $S_{lsj}^{IJ} = |A_{lsj}^{IJ}|^2$ are the spectroscopic factors [30, 32, 33]. These factors can be interpreted as a probability of finding the nucleon or cluster x in a single-particle state with quantum numbers l, s, j bound to core a or b with spin I [32]. Below, we denote the spectroscopic amplitude as A_x , where x is the nucleon or cluster with all its quantum numbers. All spectroscopic amplitudes A_x used in our calculations (Table 3) were taken from the shell model calculations reported in [13, 25, 34–37].

The wave functions of the bound states of the nucleons and dineutron clusters x in the target and projectile nuclei were obtained using the Woods-Saxon potential. The potential depths were adjusted to reproduce the experimental binding energies of the nucleons and clusters [38], while the parameters a and r_0 were fixed: $a = 0.65$ fm and $r_0 = 1.25A^{1/3}$ fm [13, 25, 39].

We adjusted only the potential parameters for the exit channels [40] while keeping the parameters for the entrance and intermediate channels as well as the spectroscopic amplitudes.

VI. REACTION CHANNELS ${}^9\text{Be}({}^6\text{Li}, {}^7\text{Li}){}^8\text{Be}_{\text{gs},3.03}$

Experimental differential cross-sections for the ${}^9\text{Be}({}^6\text{Li}, {}^7\text{Li}){}^8\text{Be}_{\text{gs}}$ and ${}^9\text{Be}({}^6\text{Li}, {}^7\text{Li}){}^8\text{Be}_{3.03}$ channels in comparison with the DWBA calculations are shown in Fig. 7. For these reaction channels, we detected the ${}^7\text{Li}$ nucleus, and the ${}^8\text{Be}$ product was considered complementary to the detected one.

Table 3. Spectroscopic amplitudes A_x for the nucleon or cluster x in the systems $A = a + x$ or $B = b + x$ [13, 25, 34–37].

A or B	a or b	x	nl_j	A_x
${}^7\text{Li}$	${}^6\text{Li}$	n	$1p_{3/2}$	-0.735
${}^7\text{Li}_{0.477}$	${}^6\text{Li}$	n	$1p_{3/2}$	0.329
${}^8\text{Li}$	${}^6\text{Li}$	2n	$1d_2$	-0.667
${}^8\text{Li}$	${}^7\text{Li}$	n	$1p_{3/2}$	-0.478
${}^7\text{Be}$	${}^6\text{Li}$	p	$1p_{3/2}$	-0.735
${}^7\text{Be}_{0.429}$	${}^6\text{Li}$	p	$1p_{3/2}$	-1.740
${}^8\text{Be}$	${}^7\text{Be}$	n	$1p_{3/2}$	-1.234
${}^8\text{Be}_{3.03}$	${}^7\text{Be}$	n	$1p_{3/2}$	0.771
${}^8\text{Be}_{3.03}$	${}^7\text{Be}_{0.429}$	n	$1p_{3/2}$	-0.655
${}^9\text{Be}$	${}^8\text{Li}$	p	$1p_{1/2}$	-0.375
${}^9\text{Be}$	${}^8\text{Be}$	n	$1p_{3/2}$	0.866
${}^9\text{Be}$	${}^7\text{Be}$	2n	$2s_0$	0.247

The potential parameters describing the elastic scattering of ${}^6\text{Li}+{}^9\text{Be}$ (Table 2) were used for the entrance channel. For the ${}^7\text{Li}+{}^8\text{Be}_{\text{gs}}$ exit channel, we also used a potential in the Woods-Saxon form with the parameters obtained by fitting the calculation results to the experimental data on the angular distributions. The parameters recommended in [41] were used as initial parameters in the fitting procedure.

The parameters of the real part of the potential for the ${}^7\text{Li}+{}^8\text{Be}_{\text{gs}}$ exit channel were the same as those for the ${}^7\text{Li}+{}^8\text{Be}_{3.03}$ exit channel. However, owing to the fact that the values of the cross-sections for the ${}^9\text{Be}({}^6\text{Li}, {}^7\text{Li}){}^8\text{Be}_{3.03}$ reaction channel are higher, we reduced the depth parameter V_W of the imaginary part for the ${}^7\text{Li}+{}^8\text{Be}_{3.03}$ exit channel. To better reproduce the shape of the experimental angular distributions, we fitted the radius parameter r_W of the imaginary part. As a result, an increased value of the radius parameter r_W was obtained for the ${}^7\text{Li}+{}^8\text{Be}_{3.03}$

exit channel. Note that our DWBA calculations reproduce the experimental data well (Fig. 7). The obtained parameters of the optical potential are listed in Table 4.

VII. REACTION CHANNELS ${}^9\text{Be}({}^6\text{Li}, {}^7\text{Be}){}^8\text{Li}$ and ${}^9\text{Be}({}^6\text{Li}, {}^8\text{Li}){}^7\text{Be}$

Similar to the ${}^9\text{Be}({}^6\text{Li}, {}^7\text{Li}){}^8\text{Be}$ reaction channel, calculations were carried out for the ${}^9\text{Be}({}^6\text{Li}, {}^7\text{Be}){}^8\text{Li}$ reaction channel, in which the proton transfer occurs from the target nucleus to the projectile nucleus, leading to the exit channel ${}^7\text{Be}+{}^8\text{Li}$. The spectroscopic amplitudes of the transferred proton used for the configurations ${}^6\text{Li}+p$ and ${}^8\text{Li}+p$ are listed in Table 3. The wave functions of the protons in the nuclei ${}^7\text{Be} = {}^6\text{Li}+p$ and ${}^9\text{Be} = {}^8\text{Li}+p$ were calculated by varying the depth of the Woods-Saxon potential to reproduce the binding energy exactly in the same manner as described in the previous section. It is worth mentioning that the binding energy of the proton p in the ${}^9\text{Be}$ nucleus is 16.9 MeV, which is comparable to the binding energy of two neutrons 2n in the ${}^9\text{Be}$ nucleus, 20.6 MeV.

The parameters of the Woods-Saxon potential for the ${}^7\text{Be}+{}^8\text{Li}_{\text{gs}}$ and ${}^7\text{Be}+{}^8\text{Li}_{0.98}$ exit channels (Table 5) were obtained by fitting the calculation results to the experimental angular distribution at fixed potential parameters for the entrance channel (${}^6\text{Li}+{}^9\text{Be}$, Table 2). The parameters reported in [42] were used as initial parameters in the fitting process.

The measured energy spectrum of ${}^7\text{Be}$ for the ${}^9\text{Be}({}^6\text{Li}, {}^7\text{Be}){}^8\text{Li}$ reaction channel is shown in Fig. 4(b). Because of the relatively low energy resolution, the low-lying excited state of ${}^8\text{Li}$ (1^+ , 0.98 MeV) is practically not resolved from the ground state. The results of the DWBA calculations for the transfer of a proton in the reaction channels ${}^9\text{Be}({}^6\text{Li}, {}^7\text{Be}){}^8\text{Li}_{\text{gs}, 0.98}$ are shown in Fig. 8. They are fairly close to the experimental angular distribution of

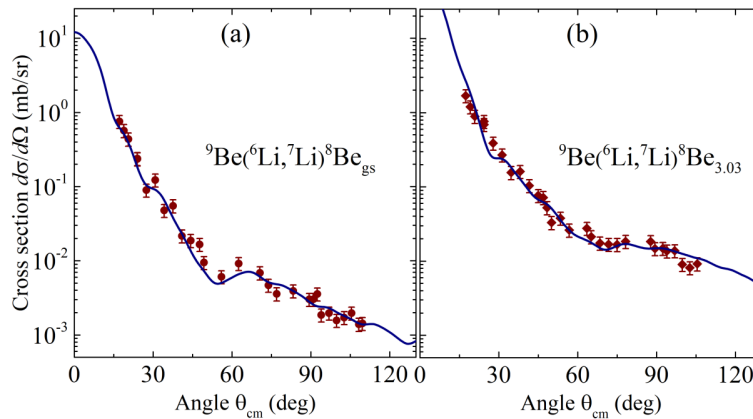


Fig. 7. (color online) Experimental angular distributions for the neutron transfer channels (a) ${}^9\text{Be}({}^6\text{Li}, {}^7\text{Li}){}^8\text{Be}_{\text{gs}}$ and (b) ${}^9\text{Be}({}^6\text{Li}, {}^7\text{Li}){}^8\text{Be}_{3.03}$ (symbols) in comparison with the calculation results (curves).

Table 4. Parameters of the optical potential (1) obtained for the specified exit channels.

Reaction channel	V_V/MeV	r_V/fm	a_V/fm	V_W/MeV	r_W/fm	a_W/fm	r_C/fm
${}^7\text{Li}+{}^8\text{Be}$	152.20	0.669	0.853	30.50	1.008	0.809	0.677
${}^7\text{Li}+{}^8\text{Be}_{3.03}$	152.20	0.669	0.853	12.36	1.388	0.809	0.677

Table 5. Parameters of the optical potential (1) obtained for the specified exit channels.

Reaction channel	V_V/MeV	r_V/fm	a_V/fm	V_W/MeV	r_W/fm	a_W/fm	r_C/fm
${}^7\text{Be}+{}^8\text{Li}_{\text{gs}}$	125.50	0.657	0.853	12.25	0.888	0.809	0.664
${}^7\text{Be}+{}^8\text{Li}_{0.98}$	115.04	0.657	0.853	12.36	0.888	0.809	0.664

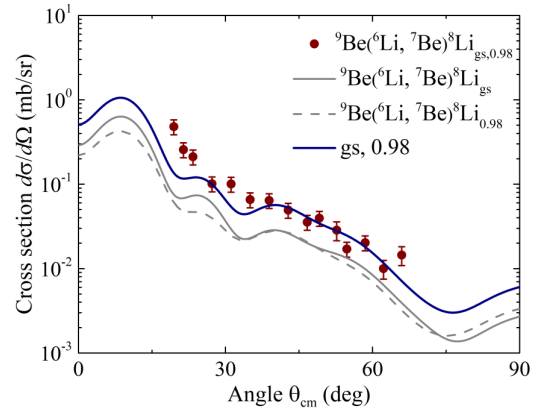
the ${}^7\text{Be}$ nucleus. The solid blue curve in Fig. 8 represents an incoherent sum of the cross-sections for the ground state and the first excited state 0.98 of ${}^8\text{Li}$. The significant contribution of the reaction channel ${}^9\text{Be}({}^6\text{Li}, {}^7\text{Be}){}^8\text{Li}_{0.98}$ in the incoherent sum of the cross-sections is consistent with the measured energy spectrum of ${}^7\text{Be}$ shown in Fig. 4(b).

The values of the experimental differential cross-sections at forward angles (three points at $\theta_{\text{cm}}=19.5^\circ-23.4^\circ$) could not be described by the theoretical curve; this may be due to the presence of a contribution from the inelastic excitation of the ${}^6\text{Li}$ projectile [43]. Nevertheless, the shape of the theoretical curve in this angular range is close to that of the experimental data.

A similar discrepancy between DWBA calculations and experimental data was observed in [43, 44]. This can be solved by adjusting the values of the spectroscopic amplitudes or reducing the imaginary part of the exit channel potential. However, in such a case, we would lose the overall agreement of the DWBA calculations with the experimental points. This fact indicates the need for more complex calculations that take into account inelastic excitations of the nuclei in the studied channels; this will be addressed in a future theoretical study.

The proton transfer, inverted with respect to the scattering angle, serves as an alternative to the two-neutron transfer mechanisms in the ${}^9\text{Be}({}^6\text{Li}, {}^8\text{Li}){}^7\text{Be}$ reaction channel [45]. Therefore, we included it in the calculations shown in Fig. 9. The one-step mechanism corresponds to the transfer of a di-neutron cluster 2n or a proton p , while the two-step mechanism corresponds to the two-step transfer of two neutrons $n-n$.

We used the same potential parameters from Table 5 for the ${}^7\text{Be}+{}^8\text{Li}_{\text{gs}}$ and ${}^8\text{Li}_{\text{gs}}+{}^7\text{Be}$ exit channels. The potential parameters obtained in Sections IV and V were used for the entrance channel (${}^6\text{Li}+{}^9\text{Be}$, Table 2) and for the intermediate channels (${}^7\text{Li}+{}^8\text{Be}_{\text{gs}}$ and ${}^7\text{Li}+{}^8\text{Be}_{3.03}$ in the calculations for the $n-n$ transfer, Table 4). The potential parameters for the exit channel ${}^8\text{Li}+{}^7\text{Be}_{0.429}$ were obtained by fitting the cross-section to reproduce the experimental data. As a starting point for seeking the potential, we used the parameters for the exit channel ${}^7\text{Li}+{}^8\text{Be}_{\text{gs}}$

**Fig. 8.** (color online) Experimental angular distribution of the reaction channels ${}^9\text{Be}({}^6\text{Li}, {}^7\text{Be}){}^8\text{Li}_{\text{gs},0.98}$ (circles) in comparison with the calculation results (curves).

(Table 4). The resulting parameters were as follows: $V_V=155$ MeV, $r_V=0.669$ fm, $a_V=0.853$ fm, $V_W=19.25$ MeV, $r_W=1.388$ fm, and $a_W=0.780$ fm.

The spectroscopic amplitudes A_x for the nucleons and dineutron clusters included in the calculations are listed in Table 3. The higher value of $A_x=0.667$ for the configuration ${}^8\text{Li}={}^6\text{Li}+2n$ compared to $A_x=0.478$ for the configuration ${}^8\text{Li}={}^7\text{Li}+n$ may favor dineutron in the cluster transfer mechanism (i.e., one-step transfer of two neutrons) compared to the two-step mechanism of neutron transfer.

The differential cross-section for the ${}^9\text{Be}({}^6\text{Li}, {}^8\text{Li}){}^7\text{Be}$ reaction channel has the form of a coherent sum of two amplitudes,

$$\frac{d\sigma}{d\Omega}(\theta_{\text{cm}}) = |f_I(\theta_{\text{cm}}) + f_{II}(\theta_{\text{cm}})|^2, \quad (6)$$

where $f_I(\theta_{\text{cm}})$ and $f_{II}(\theta_{\text{cm}})$ are the amplitudes of the one-step and two-step transfer mechanisms, respectively [29, 30]:

$$f_I(\theta_{\text{cm}}) = f_{2n}(\theta_{\text{cm}}) + f_p(\pi - \theta_{\text{cm}}), f_{II}(\theta_{\text{cm}}) = f_{n-n}(\theta_{\text{cm}}), \quad (7)$$

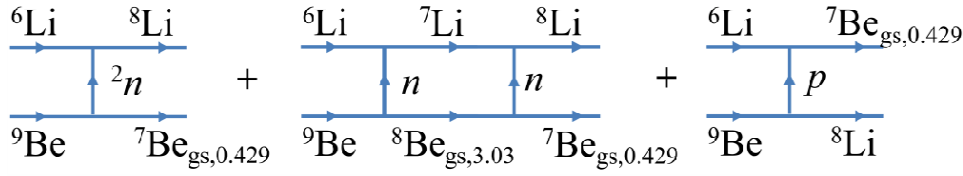


Fig. 9. (color online) Reaction mechanisms considered in the calculations.

$f_{2n}(\theta_{\text{cm}})$ and $f_p(\pi - \theta_{\text{cm}})$ are the amplitudes of the one-step transfer of two neutrons and proton, respectively; $f_{n-n}(\theta_{\text{cm}})$ is the amplitude of the two-step transfer of two neutrons. The experimental angular distribution of the ^8Li nucleus for the reaction channel $^9\text{Be}(^6\text{Li}, ^8\text{Li})^7\text{Be}$ in comparison with the calculation results is shown in Fig. 10(a). In Fig. 10(b), the DWBA calculations for each mechanism considered in the coherent sum [Eq. (6)] are presented separately:

– for one-step transfer:

- $^6\text{Li} + ^9\text{Be} \rightarrow ^8\text{Li}_{\text{gs}} + ^7\text{Be}_{\text{gs},0.429}$ ($^2n-1$ curve) – dineutron transfer included in the Sum-1 curve;
- $^6\text{Li} + ^9\text{Be} \rightarrow ^8\text{Li}_{\text{gs}} + ^7\text{Be}_{\text{gs}}$ ($^2n-2$ curve) – dineutron transfer included in the Sum-2 curve;
- $^6\text{Li} + ^9\text{Be} \rightarrow ^7\text{Be}_{\text{gs},0.429} + ^8\text{Li}_{\text{gs}}$ ($p-1$ curve) – proton transfer included in the Sum-1 curve;
- $^6\text{Li} + ^9\text{Be} \rightarrow ^7\text{Be}_{\text{gs}} + ^8\text{Li}_{\text{gs}}$ ($p-2$ curve) – proton transfer included in the Sum-2 curve;

– for two-step $n-n$ transfer:

- $^6\text{Li} + ^9\text{Be} \rightarrow ^7\text{Li}_{\text{gs}} + ^8\text{Be}_{\text{gs}} \rightarrow ^7\text{Be}_{\text{gs},0.429} + ^8\text{Li}_{\text{gs}}$ ($nn-1$ curve) included in the Sum-1 curve;
- $^6\text{Li} + ^9\text{Be} \rightarrow ^7\text{Li}_{\text{gs}} + ^8\text{Be}_{\text{gs}} \rightarrow ^7\text{Be}_{\text{gs}} + ^8\text{Li}_{\text{gs}}$ ($nn-2$ curve) included in the Sum-2 curve;
- $^6\text{Li} + ^9\text{Be} \rightarrow ^7\text{Li}_{\text{gs}} + ^8\text{Be}_{\text{gs},3.03} \rightarrow ^7\text{Be}_{\text{gs},0.429} + ^8\text{Li}_{\text{gs}}$ ($nn-3$ curve) included in the Sum-3 curve.

The angular distributions of the $^9\text{Be}(^6\text{Li}, ^8\text{Li})^7\text{Be}_{\text{gs},0.429}$ reaction channels in Fig. 10(a) have oscillations. These oscillations indicate the interference of the transfer mechanisms presented in Fig. 9. The dineutron transfer makes a relatively large contribution at forward angles, while in the range of angles 60° – 130° , the proton transfer dominates [Fig. 10(b)]. The contribution of two-step neutron transfer is negligible in the entire range of angles, which is consistent with the results of [13, 18, 46, 47].

Similar oscillations due to the interference of two-neutron and α -transfer mechanisms in the reaction $^{14}\text{C}(^{16}\text{O}, ^{18}\text{O})^{12}\text{C}$ were obtained in [45]. The incoherent

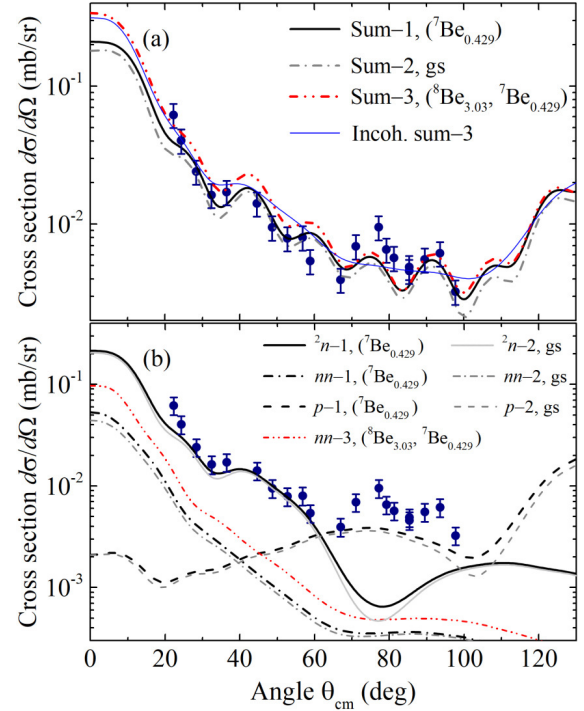


Fig. 10. (color online) Experimental angular distribution of the ^8Li nucleus for the nucleon transfer channels $^9\text{Be}(^6\text{Li}, ^8\text{Li})^7\text{Be}_{\text{gs},0.429}$ (circles) in comparison with the calculation results. The curves are the results of calculations including the excited states given in parentheses. (a) Sums of reaction mechanisms. (b) Contributions of nucleon and cluster transfer mechanisms taken into account in the calculations.

sum yields a smoother angular distribution [45, 47], as shown by the thin solid curve in Fig. 10(a). It can be assumed that the characteristic features of two-neutron transfer reactions are the domination of the one-step transfer of two neutrons and the interference of the transfer mechanisms [18, 46, 48, 49].

Note that the $^8\text{Be}_{3.03}$ state in the intermediate channel of the two-step neutron transfer provides a better description of the experimental points in the region of $\theta_{\text{cm}}=20^\circ$ – 30° ; simultaneously, the calculated cross-sections in the region of $\theta_{\text{cm}}=45^\circ$ – 70° are slightly overestimated [Fig. 10(a)]. The excitation of the $^8\text{Be}_{3.03}$ state in the intermediate channel does not have a strong effect on the calculation results for the $^9\text{Be}(^6\text{Li}, ^8\text{Li})^7\text{Be}$ reaction channel. The same results were obtained in [13] for $^9\text{Be}(^7\text{Be}, ^9\text{Be})^7\text{Be}$.

The contribution of the ${}^9\text{Be}({}^6\text{Li}, {}^8\text{Li}){}^7\text{Be}_{0.429}$ channel is insignificant, which is consistent with the excitation energy spectrum of the ${}^7\text{Be}$ nucleus [Fig. 4(a)]. However, taking into account the excitation of ${}^7\text{Be}_{0.429}$ in the exit channel improves the theoretical description of the cross-sections [Fig. 10(a)]. Note that if we exclude all excitations from the calculations, the experimental differential-cross sections will be underestimated, for example, in the regions of angles $\theta_{\text{cm}}=0-25^\circ$ and $\theta_{\text{cm}}=70-85^\circ$, which indicates the importance of considering excitations of nuclei in the reaction.

Typically, the structure of the ${}^8\text{Li}$ nucleus is considered in the two-body ${}^7\text{Li}+n$ or three-body $\alpha+n+t$ theoretical models [50, 51]. The ${}^9\text{Be}$ nucleus is usually represented as a system of two α -clusters and a neutron located with a high probability between them, i.e., $\alpha+n+\alpha$ [52-54]. However, the large contribution of the dineutron transfer to the cross-sections [Fig. 10(b)] suggests that the ${}^8\text{Li}$ and ${}^9\text{Be}$ nuclei can manifest configurations corresponding to the two-body structures ${}^6\text{Li}+{}^2n$ and ${}^7\text{Be}+{}^2n$, respectively. The contribution of the dineutron transfer mechanism in the range of angles $0-60^\circ$ is approximately five times higher than the contribution of the mechanism of two-step transfer of two neutrons [46].

VIII. CONCLUSIONS

The energy and angular distributions for the ${}^9\text{Be}({}^6\text{Li}$,

${}^6\text{Li}){}^9\text{Be}$, ${}^9\text{Be}({}^6\text{Li}, {}^7\text{Li}){}^8\text{Be}$, ${}^9\text{Be}({}^6\text{Li}, {}^8\text{Li}){}^7\text{Be}$, and ${}^9\text{Be}({}^6\text{Li}, {}^7\text{Be}){}^8\text{Li}$ channels in the ${}^6\text{Li}+{}^9\text{Be}$ reaction at an energy of 68 MeV were measured. The energy distributions of the detected nuclei reproduce the population scheme of the ground and low-lying excited states of complementary nuclei, which confirms the two-body nature of the reaction exit channels considered in this study.

The parameters of the Woods-Saxon optical potential were determined from the analysis of the experimental data on elastic scattering of ${}^6\text{Li}+{}^9\text{Be}$. The consideration of elastic scattering as well as the one- and two-step transfer reaction mechanisms led to good agreement with the experimental data on the ${}^9\text{Be}({}^6\text{Li}, {}^8\text{Li}){}^7\text{Be}$ reaction channel. It was also shown that the dineutron transfer 2n makes a larger contribution to the cross-sections of the ${}^9\text{Be}({}^6\text{Li}, {}^8\text{Li}){}^7\text{Be}$ reaction channel at forward angles compared to proton transfer and two-step transfer of two neutrons. The proton transfer makes a contribution comparable to the dineutron transfer in the range of angles $\theta_{\text{cm}}=60-130^\circ$. The contribution of two-step transfer of two neutrons is negligible in the entire range of angles. The oscillations in the angular distribution for the ${}^9\text{Be}({}^6\text{Li}, {}^8\text{Li}){}^7\text{Be}$ reaction channel indicate the interference of the transfer mechanisms. The large contribution of the dineutron transfer to the cross-sections suggests that the ${}^8\text{Li}$ and ${}^9\text{Be}$ nuclei can manifest configurations corresponding to the two-body structures ${}^6\text{Li}+{}^2n$ and ${}^7\text{Be}+{}^2n$, respectively.

References

- [1] F. M. Marqués and J. Carbonell, *Eur. Phys. J. A* **57**, 105 (2021)
- [2] Yu. E. Penionzhkevich and R. Kalpakchieva, *Light Exotic Nuclei Near the Boundary of Neutron Stability* (Singapore: World Scientific Publishing, 2022), p. 488
- [3] F. M. Marqués, *Eur. Phys. J. Plus* **136**, 594 (2021)
- [4] Z. H. Yang, Y. L. Ye, B. Zhou *et al.*, *Phys. Rev. Lett.* **131**, 242501 (2023)
- [5] H. Siwei and Y. Zaihong, *Front. Phys.* **11**, 1233175 (2023)
- [6] M. Duer, T. Aumann, R. Gernhäuser *et al.*, *Nature* **606**, 678 (2022)
- [7] J. Casal and M. Gómez-Ramos, *Phys. Rev. C* **104**, 024618 (2021)
- [8] V. K. Voitovetskii, I. L. Korsunskii, and Yu. F. Pazhin, *Sov. Phys. JETP* **20**, 1094 (1965)
- [9] A. Spyrou, Z. Kohley, T. Baumann *et al.*, *Phys. Rev. Lett.* **108**, 102501 (2012)
- [10] F. M. Marqués, N. A. Orr, N. L. Achouri *et al.*, *Phys. Rev. Lett.* **109**, 239201 (2012)
- [11] M. Cavallaro, F. Cappuzzello, M. Bondi *et al.*, *Phys. Rev. C* **88**, 054601 (2013)
- [12] B. L. Cohen and T. H. Handley, *Phys. Rev.* **93**, 514 (1954)
- [13] U. Umbelino, K. C. C. Pires, R. Lichtenthäler *et al.*, *Phys. Rev. C* **99**, 064617 (2019)
- [14] I. Tanihata, M. Alcorta, D. Bandyopadhyay *et al.*, *Phys. Rev. Lett.* **100**, 192502 (2008)
- [15] M. J. Ermamatov, F. Cappuzzello, J. Lubian *et al.*, *Phys. Rev. C* **94**, 024610 (2016)
- [16] D. K. Scott, B. G. Harvey, D. L. Hendrie *et al.*, *Phys. Rev. Lett.* **34**, 895 (1975)
- [17] J. Lubian, J. L. Ferreira, R. Linares *et al.*, *EPJ Web Conf.* **223**, 01035 (2019)
- [18] A. Parmara, Sonika, B. J. Roya *et al.*, *Nucl. Phys. A* **940**, 167 (2015).
- [19] G. M. Ter-Akopian, A. M. Rodin, A. S. Fomichev *et al.*, *Phys. Lett. B* **426**, 251 (1998)
- [20] D. T. Khoa and W. von Oertzen, *Phys. Lett. B* **595**, 193 (2004)
- [21] R. Raabe, A. Piechaczek, A. Andreyev *et al.*, *Phys. Lett. B* **458**, 1 (1999)
- [22] R. Raabe, A. Andreyev, M. Huyse *et al.*, *Phys. Rev. C* **67**, 044602 (2003)
- [23] M. Bernas, R. Devries, B. G. Harvey *et al.*, *Nucl. Phys. A* **195**, 361 (1972)
- [24] A. Chatterjee, A. Navin, A. Shrivastava *et al.*, *Phys. Rev. Lett.* **101**, 032701 (2008)
- [25] B. A. Urazbekov, T. Issatayev, S. M. Lukyanov *et al.*, *Chin. Phys. C* **48**, 014001 (2024)
- [26] S. M. Lukyanov, M. N. Harakeh, M. A. Naumenko *et al.*, *J. Phys. Conf. Ser.* **724**, 012031 (2016)
- [27] B. A. Urazbekov, A. S. Denikin, S. M. Lukyanov *et al.*, *J. Phys. G Nucl. Part. Phys.* **46**, 105110 (2019)
- [28] <http://flerovlab.jinr.ru/mavr/>, retrieved 29th June 2024
- [29] I. J. Thompson, *Comp. Phys. Rep.* **7**, 167 (1988)

- [30] <https://www.fresco.org.uk/>, retrieved 29th June 2024
- [31] D. E. Trcka, A. D. Frawley, K. W. Kemper *et al.*, *Phys. Rev. C* **41**, 2134 (1990)
- [32] G. R. Satchler, *Direct Nuclear Reactions* (New York, Oxford University Press, 1983), p. 833
- [33] J. R. Taylor, *Scattering Theory: The Quantum Theory of Nonrelativistic Collisions* (Dover Publications, 2006), p. 512
- [34] A. T. Rudchik, Yu. M. Stepanenko, K. W. Kemper *et al.*, *Nucl. Phys. A* **831**, 139 (2009)
- [35] A. T. Rudchik, A. A. Rudchik, L. M. Muravynets *et al.*, *Nucl. Phys. A* **971**, 138 (2018)
- [36] A. T. Rudchik, E. I. Koshchy, A. Budzanowski *et al.*, *Nucl. Phys. A* **609**, 147 (1996)
- [37] A. T. Rudchik, K. A. Chercas, K. W. Kemper *et al.*, *Nucl. Phys. A* **927**, 209 (2014)
- [38] I. Ciraldo, F. Cappuzzello, M. Cavallaro *et al.*, *Phys. Rev. C* **109**, 024615 (2024)
- [39] G. G. Kiss, M. La Cognata, R. Yarmukhamedov *et al.*, *Phys. Rev. C* **104**, 015807 (2021)
- [40] M. N. Harakeh, J. Van Popta, A. Saha *et al.*, *Nucl. Phys. A* **344**, 15 (1980)
- [41] J. Cook, *Nucl. Phys. A* **388**, 153 (1982)
- [42] R. Kalpakchieva *et al.*, JINR preprint, P7-2003-132
- [43] S. Micek, H. Rebel, H. J. Gils *et al.*, *Z. Phys. A-Atomic Nuclei* **328**, 467 (1987)
- [44] L. Ruby, R. V. Pyle, and Yu. -Ch. Wong, *Nucl. Sci. Eng.* **71**, 280 (1979)
- [45] W. F. W. Schneider, B. Kohlmeier, F. Pühlhofer *et al.*, *Phys. Lett. B* **46**, 195 (1973)
- [46] D. Smalley, F. Sarazin, F. M. Nunes *et al.*, *Phys. Rev. C* **89**, 024602 (2014)
- [47] S. Kahana and A. J. Baltz, *One- and Two-Nucleon Transfer Reactions with Heavy Ions in Advances in Nuclear Physics*, Vol. 9, eds. M. Baranger, E. Vogt (Boston, MA: Springer, 1977), pp. 1-122
- [48] I. J. Thompson, *Reaction Mechanisms of Pair Transfer in Fifty Years of Nuclear BCS: Pairing In Finite Systems*, edited by R. A. Broglia and V. Zelevinsky (World Scientific Publishing, 2013), p. 455-467
- [49] J. C. Zamora, J. L. Ferreira, A. Barioni *et al.*, *Phys. Rev. C* **106**, 014603 (2022)
- [50] L. V. Grigorenko, N. B. Shul'gina, and M. V. Zhukov, *Nucl. Phys. A* **607**, 277 (1996)
- [51] K. Varga, Y. Suzuki, and I. Tanihata, *Phys. Rev. C* **52**, 3013 (1995)
- [52] W. von Oertzen, M. Freer, and En'yo Y. Kanada, *Phys. Rep.* **432**, 43 (2006)
- [53] M. Freer, *Rep. Prog. Phys.* **70**, 2149 (2007)
- [54] V. V. Samarin, *Eur. Phys. J. A* **58**, 117 (2022)